



CLOSED-LOOP GUST LOADS ANALYSIS OF A SUPERSONIC FIGHTER AIRCRAFT

Arne Voß, Jan Baier

DLR - German Aerospace Center, Institute of Aeroelasticity, Göttingen, Germany, arne.voss@dlr.de

Abstract

Military supersonic fighter configurations, due to their high maneuverability requirements, are usually sized by maneuver loads. This work investigates if gusts can exert higher loads on the primary structure in terms of section loads and structural dynamic accelerations. The aeroelastic models of the free-flying aircraft are extended by a longitudinal flight control system for disturbance suppression, which is mandatory for meaningful gust analyses of longitudinally unstable aircraft. The closed-loop system is simulated in the time domain based on the aerodynamic panel methods VLM and ZONA51, applied in the subsonic and the supersonic regime, respectively. Mission profiles, certification requirements, and current research outcomes are assessed, followed by a comprehensive gust load campaign. The results suggest that the quasi-steady Pratt method is not able to accurately predict the gust loads acting on a supersonic combat aircraft, significantly falling short of the dynamic gust loads. Still, most of the gust loads stayed well within the maneuver loads envelope. However, very high accelerations (up to $\approx 100g$) due to short gust impacts are observed on the wing tips, so that mounting payloads in these areas would be difficult.

Keywords: Gust loads, closed-loop gust encounter, military fighter aircraft, panel methods, aeroelasticity

1. Introduction and Motivation

1.1. Objectives

The structural design of supersonic fighter aircraft is typically driven by their high requirements on maneuverability and the correspondingly high maneuver loads. Because of that, the design of the

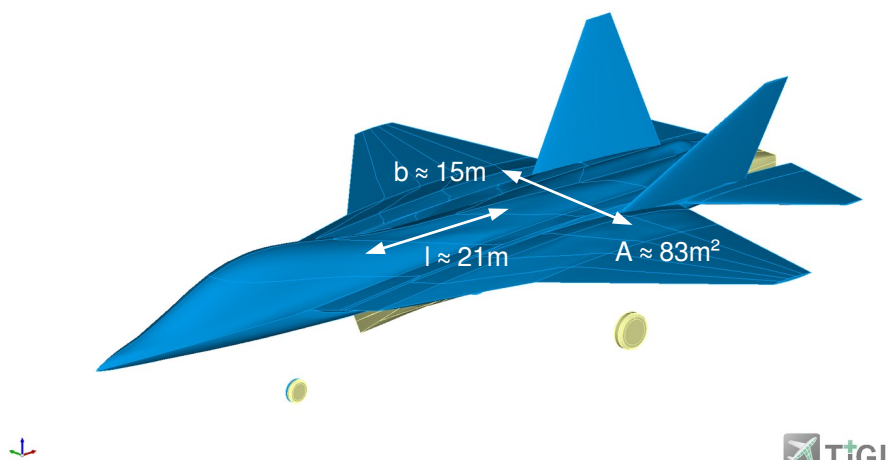


Figure 1 – The DLR Future Fighter Demonstrator (FFD), CPACS file visualized in the TtGL Viewer.

DLR Future Fighter Demonstrator (FFD) is based (so far) on maneuver loads only, calculated using CFD as well as aerodynamic panel methods. Gust loads appear to be of minor concern and are handled in a quasi-static way by military certification specifications. However, contrasting views from other publications suggest that gusts are potentially influencing the structural sizing of specific parts of the aircraft such as wingtips, attachment points and payload. To the author's best knowledge, there are only a few publications concerning the wide field of gust load analysis for supersonic fighter aircraft. Those publications give little details and provide no quantification due to the confidential nature of military projects. Because of that, results are difficult to reproduce and many questions remain open. For example, the flight profile and thus the gust load assumptions for fighter aircraft might differ from classical transport aircraft. Which gust velocities shall be considered? Is a simplified approach using Pratt's formula appropriate? Compared to maneuver loads, how important are gust loads? How large are the structural dynamic accelerations as a response to gust, for example at the wing tip? This might be important for payload attached under the wing. Finally, the aircraft is longitudinal unstable in the subsonic regime, which makes a flight controller mandatory and the gust analysis more complex as the interaction of the flight controller, the gust and the elastic aircraft has to be captured in a closed-loop simulation in the time domain. The results presented herein are a summary of the findings of the bachelor thesis of the second author [1].

1.2. Theoretical Background & Literature Review

The 1-cosine gust profile serves as a simplified representation approximating discrete atmospheric turbulence, enabling easier calculations of transient events. In a transient analysis (as e.g. in CS-25.341), the shape of the gust velocity is constructed by

$$U = \frac{U_{ds}}{2} \left(1 - \cos \left(\frac{\pi s}{H} \right) \right), \quad (1.1)$$

where U_{ds} denotes the design gust velocity and s indicates the distance of the aircraft penetrated into the gust. H denotes the gust gradient, which is the distance until the gust reaches its peak velocity.

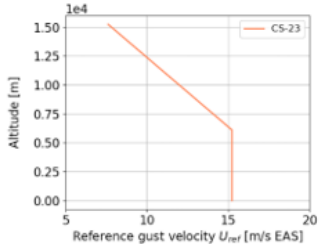
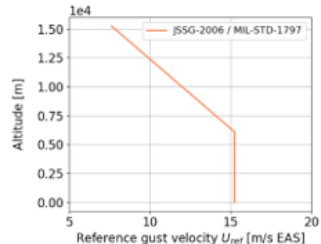
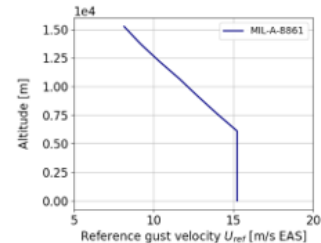
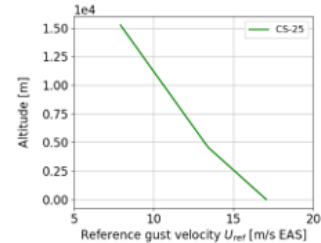
An approach to handle the discrete gust encounter in a quasi-static way is published in NACA report 1206 by Pratt and Walker [19], which is commonly referred to as Pratt's formula or Pratt method. Following Pratt, gusts are converted to an equivalent load factor N_z

$$N_z = 1.0 \pm \frac{K_g \rho_0 U_{de} V C_{L\alpha}}{2(W/S)}, \quad (1.2)$$

such that a quasi-static analysis with the given load factor N_z is sufficient. In this context, the gust gradient H is assumed as 12.5 reference chord lengths. The Pratt method is accepted by all certification authorities that require a quasi-steady simulation approach, including the certification specifications of small commuter aircraft by the European Aviation Safety Agency's (EASA) CS-23 [27], the Federal Aviation Administration's (FAA) FAR Part 23, and the certification of military aircraft under the US Navy's MIL-A-8861B [30]. It is also described as a gust method by the US Department of Defence's specification guide JSSG-2006 [28] (although the formula is not reproduced explicitly) while the US Department of Defence's MIL-HDBK-1797 [13] advises that several gust lengths shall be used, each chosen so that the gust is tuned to each of the natural frequencies of the airplane and its flight control system. That approach is also prescribed in the certification specifications of large transport aircraft CS-25 [26] and FAR Part 25 but with an emphasis on the structural dynamic response and the unsteady aerodynamics, as elaborated in the acceptable means of compliance. In addition, civil and military authorities have imposed slightly different reference gust velocities. A summary of the various regulations is given in Table 1.

Closed-Loop Gust Loads Analysis of a Supersonic Fighter Aircraft

Table 1 – Comparison of gust load certification requirements.

Name of Document (Issuing Authority)	Applicability	Last Revision	Distinctive Features	Gust Gradients	Reference Gust Velocities at V_C EAS
CS-23 (EASA, 2003) / FAR-23 (FAA, 1965)	Civil Aviation - Small and Utility Aircraft	2023 / 2023		$H = 12.5 c$	<p>From 0 to 6096 meters: -> 15.24 m/s</p> <p>From 6096 to 15240 meters: -> Linear reduction from 15.24 m/s to 7.62 m/s</p> 
JSSG-2006 (US DoD, 1998) / MIL-STD-1797 (US DoD, 1990)	Military Aviation - Entire US Military	2019 / 2006		$H = 12.5 c$ / Tuned gust	<p>From 0 to 6096 meters: -> 15.24 m/s</p> <p>From 6096 to 15240 meters: -> Linear reduction from 15.24 m/s to 7.62 m/s</p> <p>Above 15240 meters: -> $\sqrt{\sigma_{altitude}/\sigma_{15240m}}$ with $\sigma = \rho/\rho_0$</p> 
MIL-A-8861B (US DoD, 1986)	Military Aviation - US Navy	2019	Requires superposition of gust loads with $0.6 * N_z$ (Design maximum limit load factor)	$H = 12.5 c$	<p>From 0 to 6096 meters: -> 15.24 m/s</p> <p>From 6096 to 15240 meters: -> $\sqrt{\sigma_{altitude}/\sigma_{15240m}}$ with $\sigma = \rho/\rho_0$</p> 
CS-25 (EASA, 2003) / FAR-25 (FAA, 1965)	Civil Aviation - Large Transport Aircraft	2023 / 2023	Knockdown of reference gust velocities by Flight profile alleviation factor F_g	Sufficient number of gust gradients H in range of 9 – 107 meters	<p>From 0 to 4572 meters: -> Linear reduction from 17.07 m/s to 13.41 m/s</p> <p>From 4572 to 15240 meters: -> Linear reduction from 13.41 m/s to 7.92 m/s</p> 

The gust load requirements in the military specifications are of problem-solving nature, accepting simplified approaches rather than performing a more physical and thus more precise load prediction. The problem is rooted in the derivation of the Pratt formula that adversely affect its accuracy. The alleviation factor K_g , which predicts the peak acceleration relative to the reference aircraft B-247, is estimated using empirical data from the 1940s. This prediction assumes that the pitching motion of the considered aircraft is influenced by accelerations in a similar way to the reference aircraft. Therefore, the method is most precise when applied to aircraft with similar characteristics as those used in the derivation of the Pratt formula. In addition, Handojo and Klimmek [8] demonstrated that quasi-static analysis with the Pratt method yields acceptable wing root bending moments but may not accurately predict the wing root torsion moment when compared to dynamic simulations. The overall impression is that the military specifications lag behind the civil specifications, which indicates that gusts are historically only of minor importance for such aircraft. Now, it appears to be common practice in the defense industry to use more recent civil certification methods such as dynamic simulation of gust loads.

Looking at the gust encounter of fighter aircraft, Becker [3] (Messerschmitt-Bölkow-Blohm) reports that especially short gusts can lead to very high accelerations. In his case, a 18m gust excites the second wing bending frequency, leading to vertical accelerations at the wing tip which are a multiple times higher compared to the acceleration of the overall aircraft. This is confirmed by Luber et al. [11], (Daimler Benz Aerospace), who provide the additional information that the second symmetric wing bending is at 20.33 Hz, although it is not clear for which mass case. A similar finding is reported by Chapman [6] (British Aerospace, Military Aircraft Division), who states that a short gust can excite the fundamental wing bending or torsion modes, so that parts of supersonic combat aircraft can be designed by gust induced loading rather than manoeuvre induced loads. As these publications are from industrial companies, any quantification is missing, which is understandable and due to the confidential nature of military projects. Also, these publications only use subsonic aerodynamic panel methods. To the author's best knowledge, there is no publication with respect to the application of the supersonic ZONA51 panel method to the gust encounter of a fighter configuration.

Note that MIL-A-8861B and JSSG-2006 also request the combination of maneuver and gust loads, for example 0.6 times the design maximum symmetrical flight limit load factor plus a 7.62 m/s vertical gust. Within the scope of this work, only the pure gust encounter is addressed.

Maximum speed	VC = Ma 2.0 at 36,000 - 50,000 ft VD = Ma 2.3 at 36,000 - 50,000 ft
Maximum altitude	50,000 ft
Mission radius	550 - 700 NM
Mass	30.0 – 36.0 t maximum take-off mass (MTOM)
Payload	air 2 air mission: 1820 kg (internal) optional: 8000 kg (internal + external)
Agility	Load factor Nz = -3.0 ... +9.0 with basic flight design mass (BFDM)
Longitudinal Stability	Subsonic: unstable, supersonic: stable
Control surfaces	All-movable horizontal tail planes (pitch) Ailerons along trailing edge (roll) Two vertical tail planes with rudder (yaw)

Table 2 – Overview of DLR Future Fighter Demonstrator (FFD) key design parameters.

2. Aeroelastic Modeling

The DLR Future Fighter Demonstrator (FFD) is a highly agile, two-seated aircraft with twin-engines with reheat and a targeted maximum take-off mass between 30.0 – 36.0 t. An overview of the key parameters is given in Table 2. Within the project, the DLR Institute of System Architectures in Aeronautics has taken the task to devise a conceptual design that fulfills the top level aircraft requirements (TLARs) which were defined before in a project-internal specification document. A special software and a knowledge based approach is used that relies on empirical correlations from a multitude of disciplines. They are combined with an automated constraint and mission capability analysis. More details on that approach are given by Mancini et al. [12]. The resulting conceptual design is then enhanced with a more detailed aerodynamic shape [21] in a manual step by the DLR Institute of Aerodynamics and Flow Technology. The resulting geometry of the FFD is shown in Figure 1. In parallel, an engine is designed by the DLR Institute of Propulsion Technology. To enable the exchange of information within the project, the Common Parametric Aircraft Configuration Schema (CPACS) is used. For the set-up of the aeroelastic simulation models, which include the structural model, the mass models, the aerodynamic panel model, the geometry for CFD meshing, and the aero-structural coupling model, the parametric model generator ModGen [9] is used, which is developed at the DLR Institute of Aeroelasticity.

2.1. Aerodynamic Model

To obtain aerodynamic pressure distributions in the frequency domain, the doublet lattice method (DLM) [22] is used for the subsonic regime and the ZONA51 method [7,10] for the supersonic regime. For both methods, the lifting surfaces are discretized using a panel mesh shown in Figure 2. The mesh consists of 1112 panels and four control surfaces. The left and right horizontal tail planes (HTP) are all-movable and are used for both pitch and roll control while the left and right vertical tail planes (VTP) have a conventional rudder. Although the aerodynamic methods consider the lifting surfaces as flat plates, it is possible to add a correction for airfoil camber and wing twist, which is indicated by the color in Figure 2. Note that currently a (preliminary) symmetric airfoil is used for the wings, so the main influence of this correction can be seen in the fuselage region. Following Watson [25], linear aerodynamics are adequate for calculating design loads, as the highest loads typically arise at high-speed conditions where the aerodynamics remain within the linear regime. To establish if this assumption holds true, a comparison with results obtained with CFD is presented in [23].

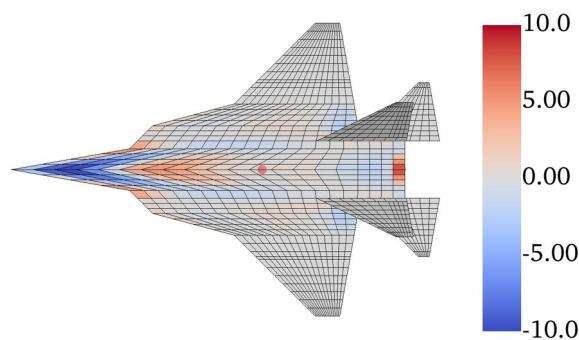


Figure 2 – Aerodynamic mesh for DLM & ZONA51 incl. correction for camber and twist (indicated by color).

2.2. Structural and Mass Model

The first aim of the structural model is to adequately represent the overall structural dynamic characteristics of the aircraft (e.g. wing bending and twist), which are important for aeroelastic analyses. Therefore, all primary structural elements, including the spars, ribs, upper and lower skin, are modeled using shell elements (CQUAD4, PSHELL and MAT1) and are completed by spar caps, stiffeners and stringers, using beam elements, to avoid local buckling and to provide a more realistic structure. For the wing, a structural layout with three main spars and multiple ribs, orientated in flow direction, is devised. Similar to the wing, the horizontal and the vertical tail are modeled and attached to the rear fuselage using rigid body elements (RBE3). Not included in the structural model are the air intakes and the cockpit. The rationale behind this decision is that although both components are large, they don't belong to the primary, load-carrying structure and their influence on the overall structural dynamic behavior of the aircraft is neglected, though their mass and moment of inertia is considered. The resulting MSC.Nastran finite elements model is shown in Figure 3, has a size of ~25.000 degrees of freedom (DoF) and includes 4292 grid points, 4754 shell elements and 4096 beam elements.

The mass model includes the structural masses, system masses, fuel masses and payload. The structural masses are derived from the skin thickness and/or the cross section of the beam elements combined with the material density. They are completed by mass estimates for the components not included in the structural model (e.g. air intakes and cockpit). For the aircraft systems, empirical mass estimates are available from the conceptual design. Also, a total of 9909 kg of fuel is estimated, which is distributed over four fuel tanks per side and included in the mass model with both mass and inertia properties. Finally, a design payload of 1820 kg for an air to air missions is taken into account, distributed over three weapon bays. Different combinations of fuel and payload masses are considered using four mass configurations summarized in Table 3. The configurations M1 to M4 are selected in such a way that they roughly represent the different mass cases that occur during a mission of the aircraft, ranging from the heaviest mass case M1 at take-off to the lightest mass case M4 just before landing. Mass case M2 corresponds to the basic flight design mass (BFDM) where the aircraft is required to achieve its full performance. Mass case M3 is similar to M2 but without payload.

Table 3: Overview of mass configurations.

Mass case	Fuel	Payload	Mass	CG _x [m]
M1 (MTOM)	100%	Yes	26.2t	4.82
M2 (BFDM)	70%	Yes	23.2t	4.77
M3	70%	No	21.4t	4.87
M4 (OEM)	0%	No	14.5t	4.82

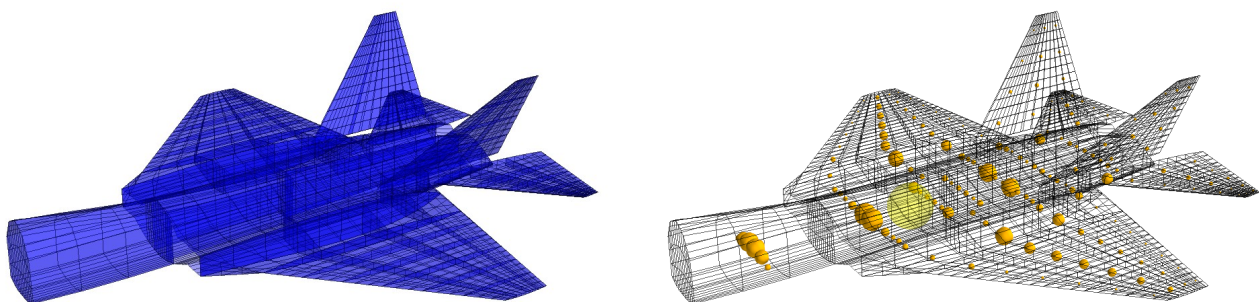
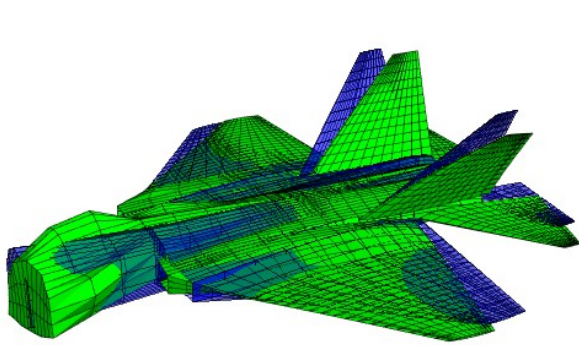


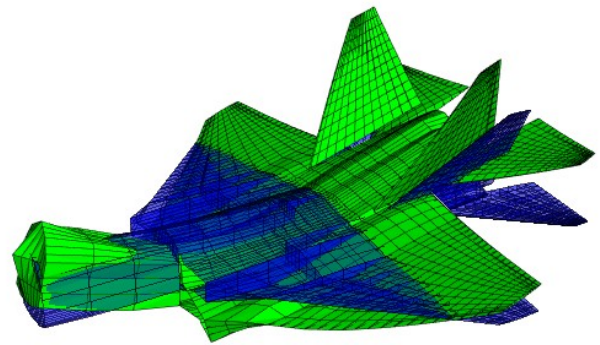
Figure 3 – Structural and mass modeling.

The combination of structural and mass model yields the structural dynamic properties in terms of eigenfrequencies and mode shapes. For the gust analysis, a modal reduction is applied, including the first 14 modes, which correspond to a highest frequency of 30 to 40 Hz, depending on the mass configuration. As an example, the first six mode shapes of mass configuration M2 are visualized in Figure 4.

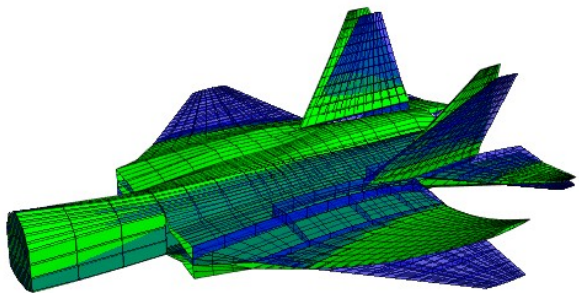
The first two elastic modes are the lateral and longitudinal fuselage bending, starting at 7.8 and 7.9 Hz for, followed by the asymmetric and symmetric wing bending at 8.8 and 9.6 Hz. Note that this is



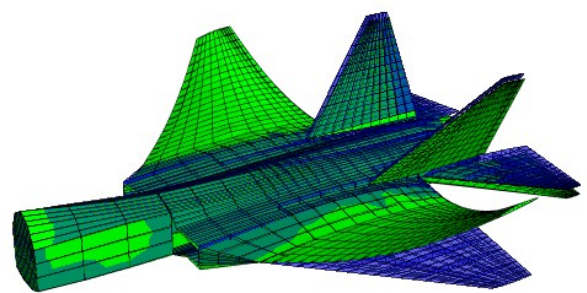
Lateral fuselage bending, 7.8 Hz



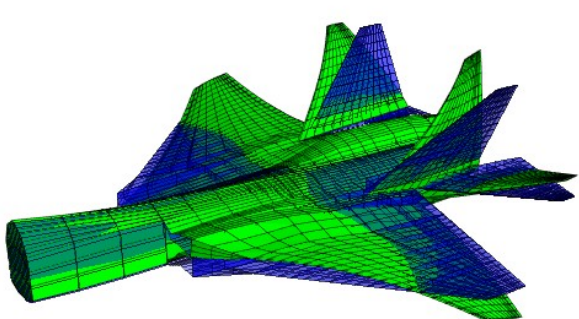
Longitudinal fuselage bending, 7.9 Hz



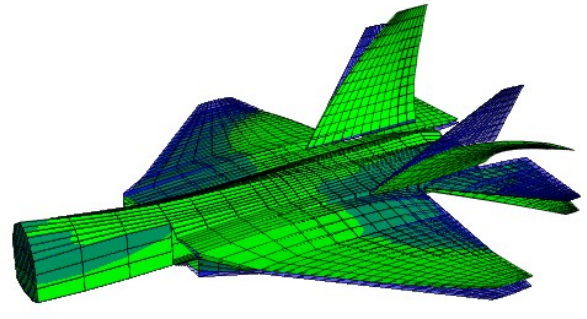
Asymmetric wing bending, 8.8 Hz



Symmetric wing bending, 9.6 Hz



Asymmetric wing torsion, 12.7 Hz



Tail rock + asym. wing bending, 14.7 Hz

Figure 4 - Overview of first elastic frequencies and mode shapes for mass configuration M2.

relatively high when compared to a typical transport type aircraft (first wing bending often in the range of 1 to 2 Hz), which can be explained by the stiff structure (sized to withstand maneuver load cases with a load factor $N_z = -3.0 \dots +9.0$), the small aspect ratio as well as the large cross sections of the wing. The next mode is an asymmetric wing torsion at 12.7 Hz, followed by a tail rocking mode combined with wing bending in opposite direction at 14.7 Hz. Luber et. al. [11] show a comparable range for the eigenmodes of a supersonic fighter aircraft, which supports the plausibility of this model.

2.3. Simplified longitudinal flight control system

Similar to other fighter aircraft such as the Eurofighter [4], the DLR FFD is designed to be unstable in the subsonic regime, providing enhanced agility. This instability results from the location of the aerodynamic center (AC), positioned slightly in front of the center of gravity (CG), making the aircraft marginally unstable (about $-4.8 \%MAC$, depending on Mach number and mass configuration). In the supersonic regime, the AC moves rearwards and is located behind the CG, resulting in a stable configuration. The reaction of the naturally unstable aircraft to a gust is much stronger and self-intensifying (divergence) than the reaction of a stable aircraft and more difficult to control. This also means that for a meaningful gust analysis, a longitudinal flight controller is mandatory.

The proposed longitudinal flight controller is shown in Figure 5 and is simplified in the sense that it is developed with a focus on the disturbance suppression due to a gust encounter. Other aspects of the electronic flight control system (EFCS) are disregarded due to the scope of this work. However, the controller design will be based on the certification requirements for control systems of military combat aircraft MIL-DTL-9490E [31] and take into account the best practices for flight control design of combat aircraft compiled by NATO [15]. According to Stevens and Lewis [20], either the angle of attack α or load factor N_z are the most suitable reference inputs to adjust longitudinal stability of agile combat aircraft. (Side note: When flying at low speeds, the maximum angle of attack limits the achievable vertical load factor since the aircraft would stall before reaching its limit. Meanwhile, at high speeds, the airframe would first reach the structural load limit before the airplane stalls. The intersection of the angle of attack and the load factor limit is commonly referred to as the corner point of the V-n diagram, which coincides with the maximum maneuver speed V_A .) In this work, the pitch angle Θ substitutes the angle of attack α as reference input. Employing three cascaded loops, the stability augmentation system is designed with the following structure. The pitch angle Θ_{comm} or the load factor $N_{z,comm}$ are pilot stick commands or stem from a higher level flight path control system and are input for the attitude control loop. It incorporates a PI controller, where the proportional component increases the aircraft's stability, and the integral component provides stationary accuracy by

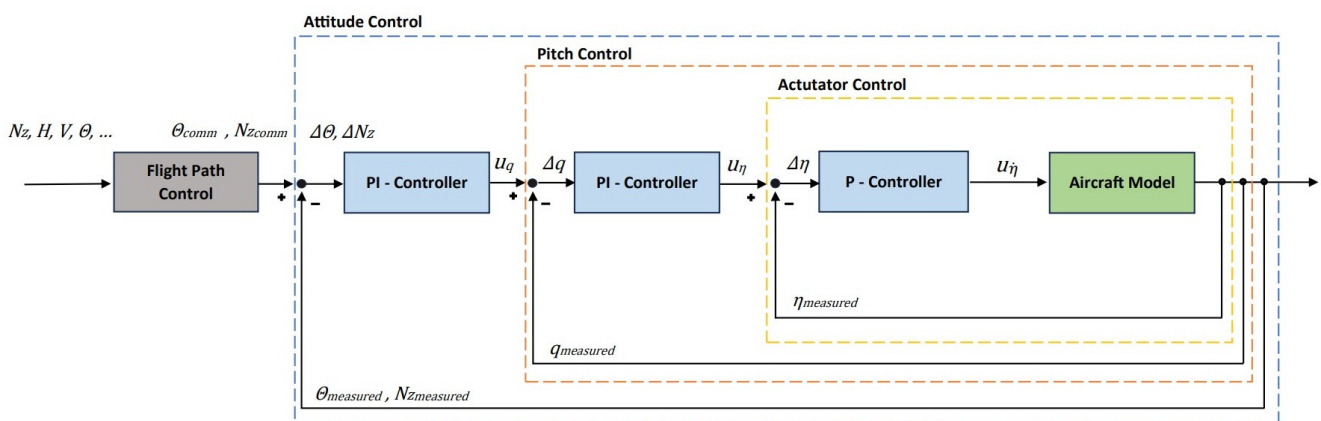


Figure 5 – Proposed longitudinal flight control system.

compensating for gain scheduling errors. The pitch control loop adjusts and dampens the pitch rate q by a PI controller, which receives the error between the commanded and measured pitch rates u_q and q_{measured} . The resulting command provides the required elevator deflection u_η to obtain the desired pitch rate u_q . The actuator control loop then adjusts the deflection rate $\dot{\eta}$ of the control surfaces by comparing the commanded deflection u_η from the pitch controller to the current elevator deflection η_{measured} . The error is amplified by a gain in the proportional controller and both min./max. deflection and deflection rate limit filters are implemented. To resemble the actual behavior of modern combat aircraft, this work adopts the deflection rate limits of the actuators integrated in the Lockheed Martin F-22 Raptor [2,14], which is a current-generation combat aircraft with comparable capabilities to the DLR Future Fighter Demonstrator. For the horizontal tail, the deflection limits are set at $\eta = -25^\circ \dots +30^\circ$ and with a rate limit of $\dot{\eta} = \pm 60^\circ/s$. Note that over-optimistic deflection rates, which do not reflect the current capabilities of combat aircraft, can produce misleading results.

The control gains $K_{P,\text{attitude}}$, $K_{I,\text{attitude}}$, $K_{P,\text{pitch}}$, $K_{I,\text{pitch}}$ and $K_{P,\text{actuator}}$ are determined by an iterative optimization approach employing a genetic algorithm. This approach ensures a good exploration of the parameter range and eliminates the influence of human judgment. The procedure involves simulating the entire system subjected to a step-input in the linearized state space form and at all operational points. Figure 6 shows a schematic sketch of the resulting step response compared to the desired response. The desired response is based on the optimal damping $\zeta_{\text{opt}} = \sqrt{2}/2$ and optimal frequency $\omega_{\text{opt}} = 3 \text{ rad/s}$ of a class IV, category A, level 1 aircraft specified by MIL-F-8785C [32]. The genetic algorithm performs iterations on different gains to determine the optimal values such that the area between the two curves is minimized, with additional penalties for oscillating behavior and slow rise time. Gust load alleviation techniques using active control (as e.g. for passenger transport aircraft) are not considered in this context. For a more detailed discussion of the derivation of the control gains, please see section 4 in [1]. The stability of the controller was evaluated by inspecting the behavior at different operational points across the envelope. A reduction of the sampling rate of the controller was performed, which is similar to a time delay of the sensor signals, e.g. due to internal processing times. A reduction down to 10.0 Hz (equivalent to a 100 ms delay) showed no significant loss in performance. To avoid numerical problems e.g. due to stepped actuator commands, the

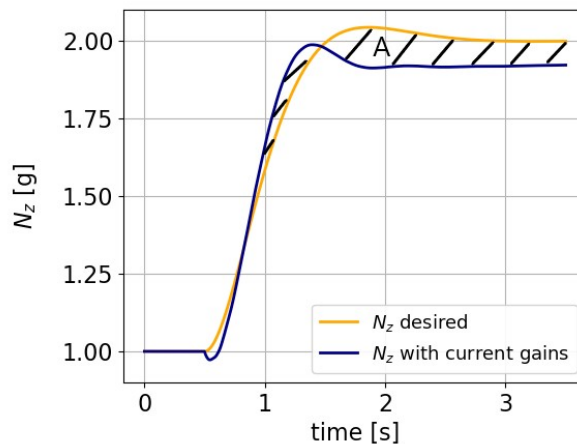


Figure 6 – Comparison of aircraft behavior to a step input with current gains compared to the ideal behavior.

controller will run at every time step in the following simulations, where a Adams-Bashforth scheme [5] with variable step size is used for the time integration.

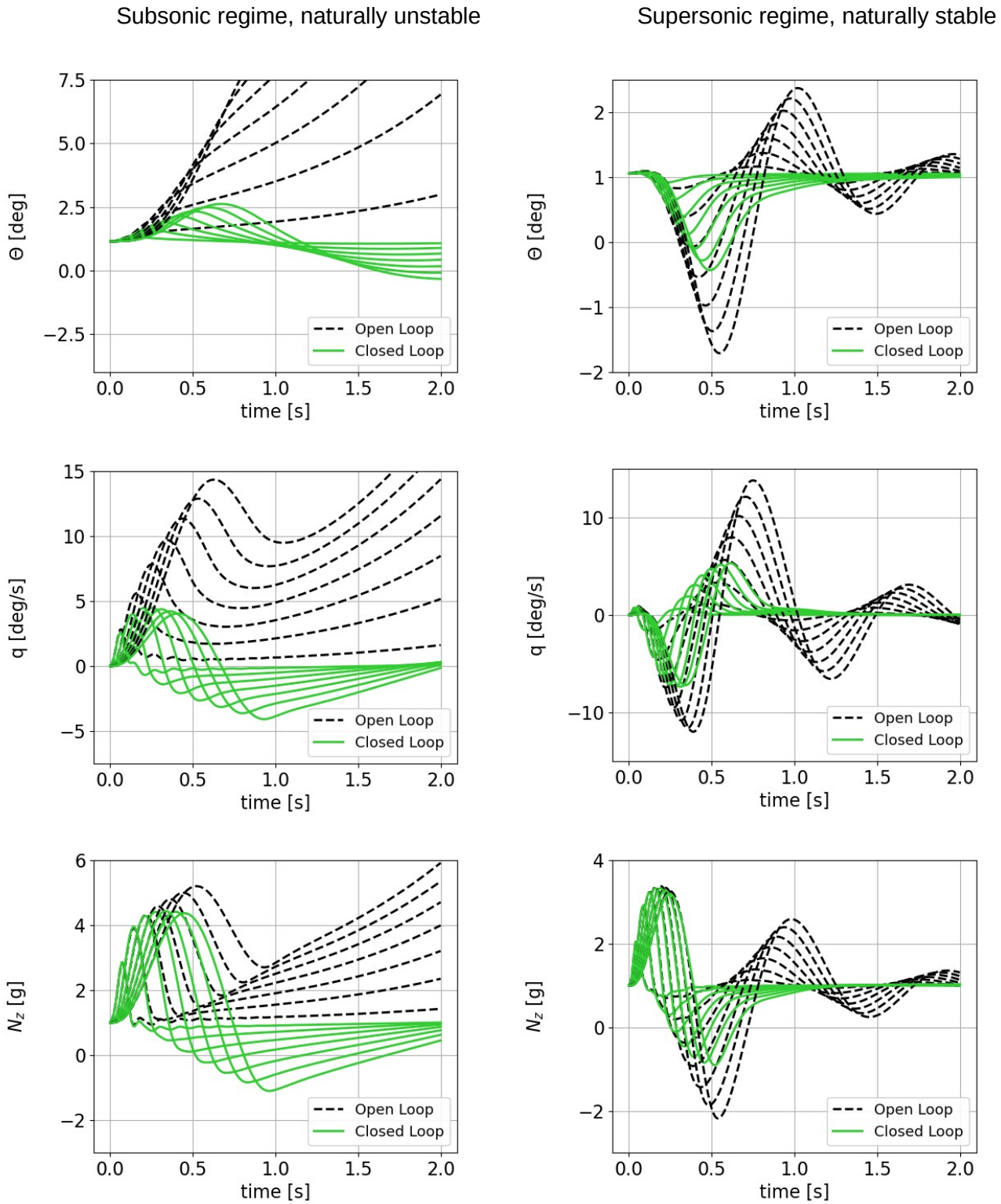


Figure 7 – Comparison of the open loop and close loop responses for different gust impacts.

Figure 7 shows the response of the aircraft to a gust encounter at two selected operational points in the subsonic (on the left) and the supersonic regime (on the right). The green lines show the response of the closed loop system while the dashed black lines show the open loop responses for reference. Looking at the Euler angle Θ and the pitch rate q , it can be seen that the controller stabilizes the naturally unstable aircraft efficiently in the subsonic regime and also greatly dampens the response of the naturally stable configuration in the supersonic regime. The load factor N_z , shown in the two bottom plots, underlines the necessity of the controller for a meaningful gust loads analysis - otherwise the loads would be very unrealistic due to the diverging behavior of the aircraft. Figure 8 shows that only moderate deflections of the horizontal tail plane are needed to stabilize the aircraft. Surprisingly, a stronger control action can be seen for the stable configuration, where the bandwidth of the deflection is slightly higher with $\Delta\eta \approx 5^\circ$ compared to a $\Delta\eta \approx 4^\circ$ for the subsonic cases. One explanation could be that the absolute moments required to rotate the aircraft are smaller for the subsonic case, where the stability margin is $-4.8\% \text{MAC}$ compared to $+12.6\% \text{MAC}$ in the supersonic case. In all cases, the deflections stay well below the imposed limits.

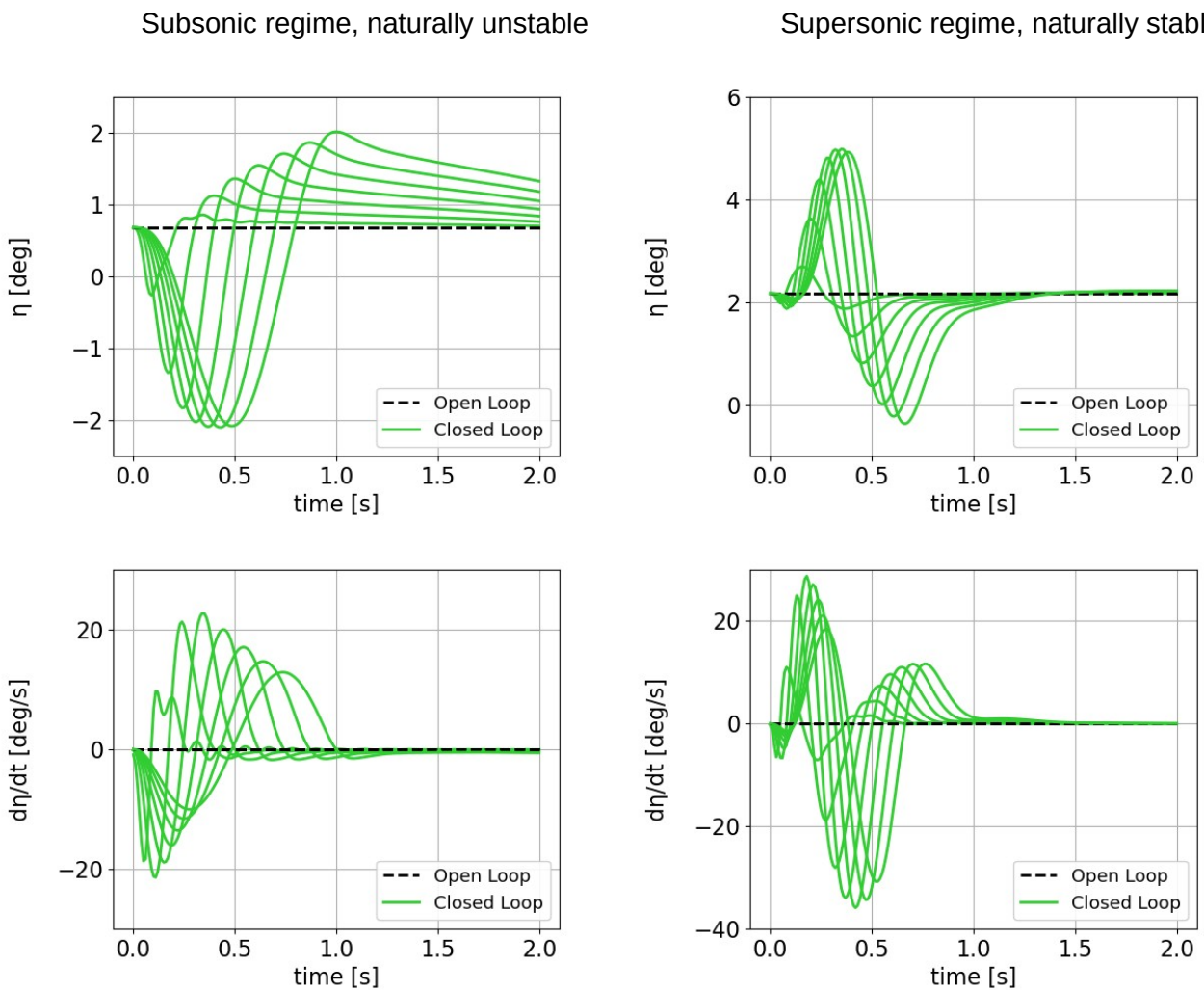


Figure 8 – Comparison of required control surface deflections and deflection rates.

3. Loads Analysis

3.1. Gust Load Case Selection

The flight envelope of military aircraft shown in Figure 9 and defined in MIL-A-8860B [29] and MIL-A-8861B [30] follows a similar approach compared to the flight envelope of civil aircraft defined for example in CS-25 [26]. In this work, the military flight speeds V are indicated with a subscript and the civil flight speeds with a capital character. Gust analyses will be performed at the velocities V_A , V_C and V_D . At the dive speed V_D , the dynamic pressure and the mach number are the highest but only half the gust magnitude has to be considered, while at the design cruising speed V_C , the full gust magnitude is prescribed. Each dot in Figure 9 marks an operational point, so that all edges and corners of the envelope are covered, plus some intermediate points. These operational points are then combined with all four mass cases detailed in Table 3. As already described in the introduction, to the authors best knowledge, no publication offers a comprehensive gust loads analysis covering a wide range of relevant parameters for the operating points of a fighter aircraft. Most investigations typically concentrate on a few selected points to reduce computing power. Still, as Neubauer and Günther [16] pointed out, not only the corner cases of the flight envelope but also the operational points within the envelope should be analyzed as peak loads occur occasionally within the envelope.

The literature review in section 1.2 discussed how the applicable certification requirements, despite dealing with the same problem, frequently differ when it comes to the reference gust velocity they are based on. This raises the question: why isn't there a universally applicable reference gust velocity for all simulation methods? One answer is that the reference velocities are specifically adapted for the simulation method in question, and selecting alternative reference gust velocities would yield inaccurate outcomes for the methods applied. Although mixing the requirements is not a good idea, the gust load assumptions given in CS-25 need some adjustments. First, the prescribed range of gust gradients $H = 9 \dots 107 \text{ m}$ is extended up to $H = 2 \dots 177 \text{ m}$, which corresponds to Luber's proposal of gust gradients up to 25 reference chord lengths [11]. The next assumption is that the scaling of the gust velocity by the sixth root of the gust gradient can be extrapolated beyond $H = 107 \text{ m}$, which means that the design gust velocity U_{ds} will exceed the prescribed reference velocity $U_{ref} = 17.07 \text{ m/s}$ as visualized in Figure 9. Additionally, CS-25 incorporates a flight profile alleviation factor F_g , which decreases the gust velocities by accounting for the particular mission profile of the considered aircraft configuration. For the FFD, the specified formula yields $F_g \approx 0.7$, which is a rather

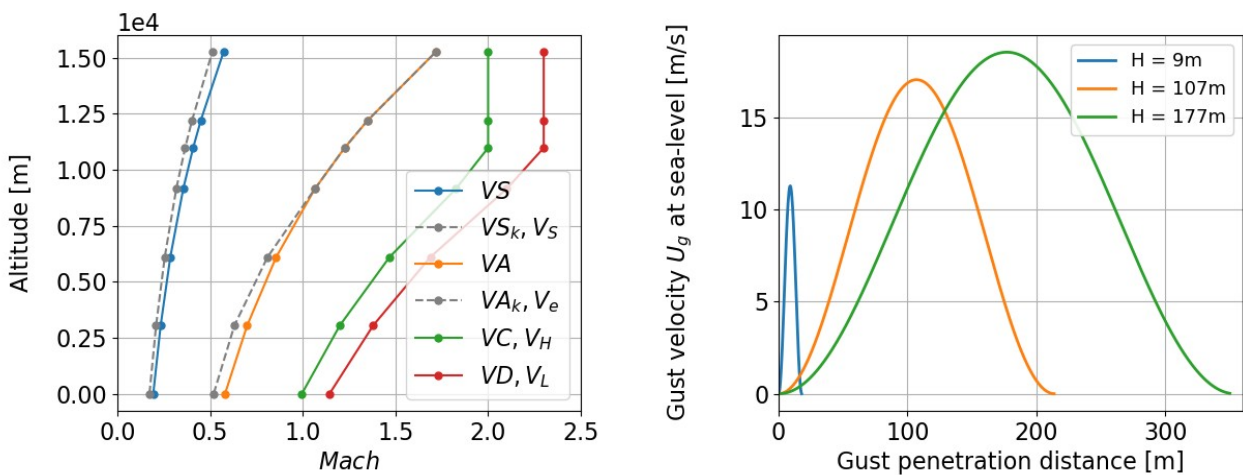


Figure 9 – Proposed design speeds and gust velocity profiles.

low value and comparable to a long range configuration, which spends most of the flight time at high altitudes. Combat aircraft are expected to operate on a range of mission profiles at variable altitudes and speeds, making an alleviation of reference gust velocities rather implausible. Therefore, in absence of a more rational approach, the flight profile alleviation factor is selected to $F_g = 1.0$ for this investigation, which means that the aircraft flies at all altitudes equally.

3.2. Gust Loads Analysis

In the following, the section loads due to the gust encounter are analyzed in terms of bending and torsional moments M_x and M_y at two monitoring stations at the wing root and at a mid-wing location. Often, sizing loads result from a combination of two quantities, so the typical approach to analyzing loads is to compare two-dimensional envelopes. From each load case, slices are extracted from the time domain simulation at the min./max. peaks of each quantity, resulting in one dot in the loads envelopes shown below. Finally, the convex hull (dashed line) is constructed and used to identify the sizing load cases. Note that the meaning of the colors changes from one Figure to the other, but will be explained in the following.

In Figure 10, the loads from the sub- and the supersonic regime are compared, because not only the Mach numbers are different but also different aerodynamic methods (DLM and ZONA51) are employed. From the two plots, it is evident that the highest bending moments M_x are due to the supersonic gusts while the highest torsional moments M_y are caused by the subsonic gusts. Generally, the envelope of the subsonic load cases is rotated in clock-wise direction with respect to the subsonic load cases. This could be explained by the large range of travel of the aerodynamic center, with a location further rearwards for supersonic speeds compared to subsonic speeds and corresponds to previous observations concerning maneuver loads [24].

To investigate the influence of the gust lengths, the loads are divided in four different sets and compared in Figure 11. The CS-25 set includes all gusts with the gradients $H = 9 \dots 107 \text{ m}$ requested by CS-25. As described in section 3.1, that range was extended and the shorter and longer gusts are in the Short and Long set. Finally, the Pratt set comprises a single gust gradient of exactly 12.5 spatial chords like the one used in the quasi-steady Pratt method. From the envelopes it can be concluded that the gust gradients necessary for the CS-25 type certification are adequate for supersonic combat configurations similar to the FFD. When computational power is limited, a first, rough estimate of peak loads could be obtained by considering the a gradient of 12.5 spatial chords. The shorter gusts are not relevant in terms of loads and the sizing of the overall aircraft, but become more important on a local level, which will be demonstrated in section 3.3.

Finally, Figure 12 compares the gust loads to the maneuver loads adopted from a previous work by the author [24]. It can be seen that the gust loads are significantly smaller than the maneuver loads - the envelope is approximately half in size. At the same time, the transient 1-cos gusts do indeed produce higher negative wing bending moments M_x than maneuvers (left side of the envelope), as gusts show symmetry around the horizontal level flight. However, maneuvers lack this symmetry as they can range from $N_z = -3.0 \dots +9.0$. Although the negative loads are only a third of the observed positive wing bending moments M_x , they could effect the design and material selection, for example when the upper and lower skin of an aircraft wing are made of materials with different tensile strength or if buckling is the limiting sizing criterion on the lower skin. Apart from that, these findings support the outcome of the literature review in section 1.2, which indicate that gust loads only have a minor impact on the sizing of the overall primary structure of supersonic combat aircraft.

Closed-Loop Gust Loads Analysis of a Supersonic Fighter Aircraft

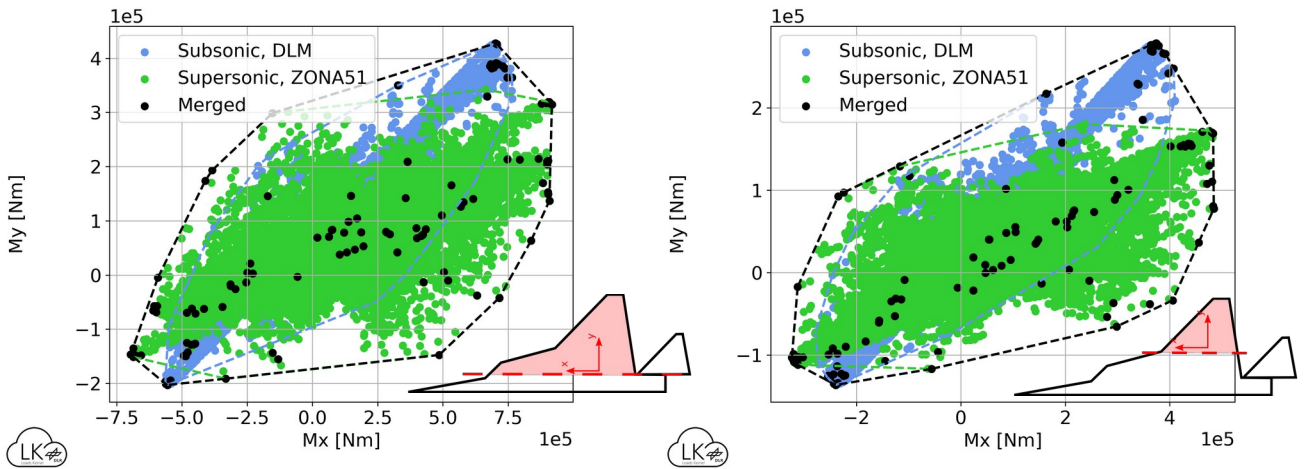


Figure 10 – Comparison of the transient 1-cos gust loads in the sub- and supersonic regime.

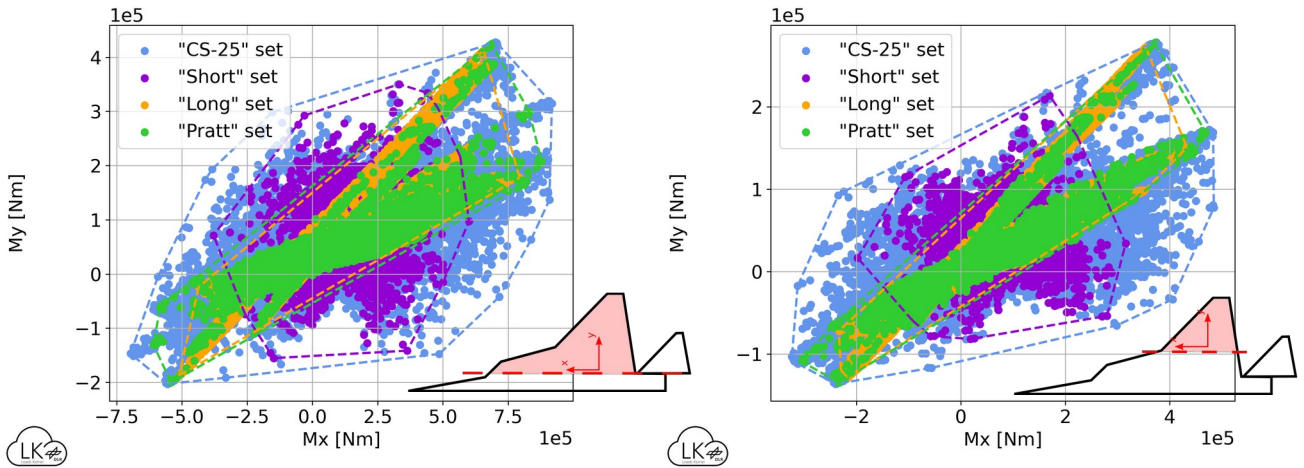


Figure 11 – Comparison of different gust gradient sets for the transient 1-cos gust analysis.

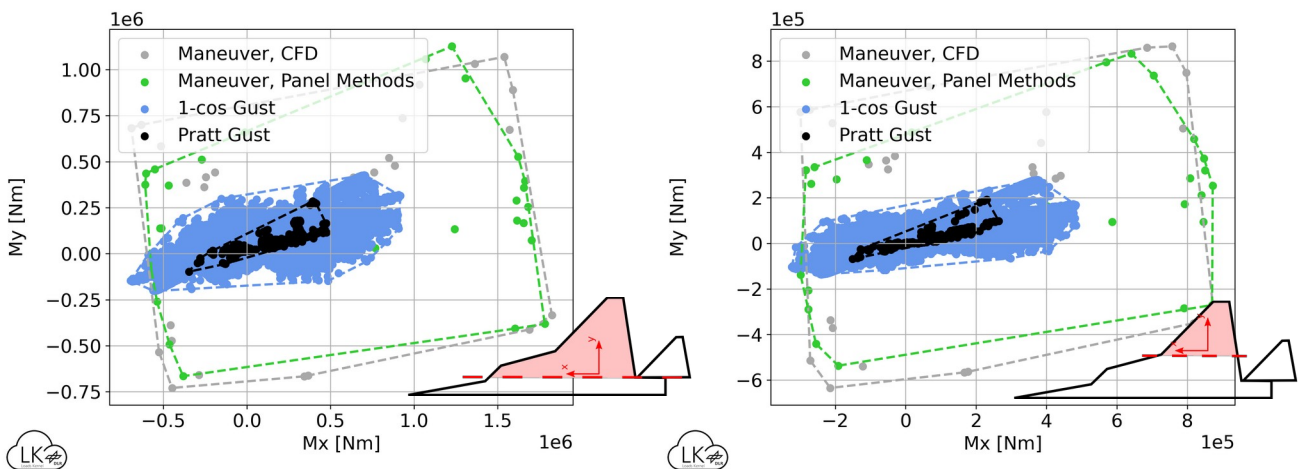


Figure 12 – Comparison of maneuver loads and gust loads.

3.3. Structural dynamic accelerations

Although short gusts showed only moderate bending and torsional moments M_x and M_y , high structural dynamic accelerations are reported in the literature. Therefore, Figures 13 and 14 show the accelerations at various locations on the aircraft. The gust load cases are filtered in such a way that the red and the blue lines show the gust encounter with the min. and max. acceleration per location. This means that the two curves may belong to completely different load cases, only the gust gradient is the same. In addition, only positive gusts (from the bottom) are considered, which removes the symmetry with respect to the horizontal level flight and allows the identification of the negative peak accelerations due to a positive gust. Note that in some cases, the lines for min. and max. acceleration coincide. Finally, the two dashed, gray lines show the acceleration close to the center of gravity as a reference.

Figure 13 displays the accelerations with a gust gradient of $H = 56 \text{ m}$, which induced the peak wing root bending moments M_x during the 1-cos gust load simulation. For this gust gradient, the accelerations at the center of gravity reach about $+7.3g$ and $-2.7g$. In the cockpit, the accelerations are very similar due to the vertical structural members running as shear walls from the rear to the front fuselage. For the positive gusts, these accelerations are still within the range of the maneuver load factor with $N_z = -3.0 \dots +9.0$. For a negative gust (not shown in the plots), the accelerations would be $-5.3g$ and would exceed that range clearly. Looking at the locations along the wing, the structural dynamic behavior increases as the wing is excited by the gust. Especially at the wing tip, an oscillation of much higher frequency than the rigid body motion of the aircraft can be seen.

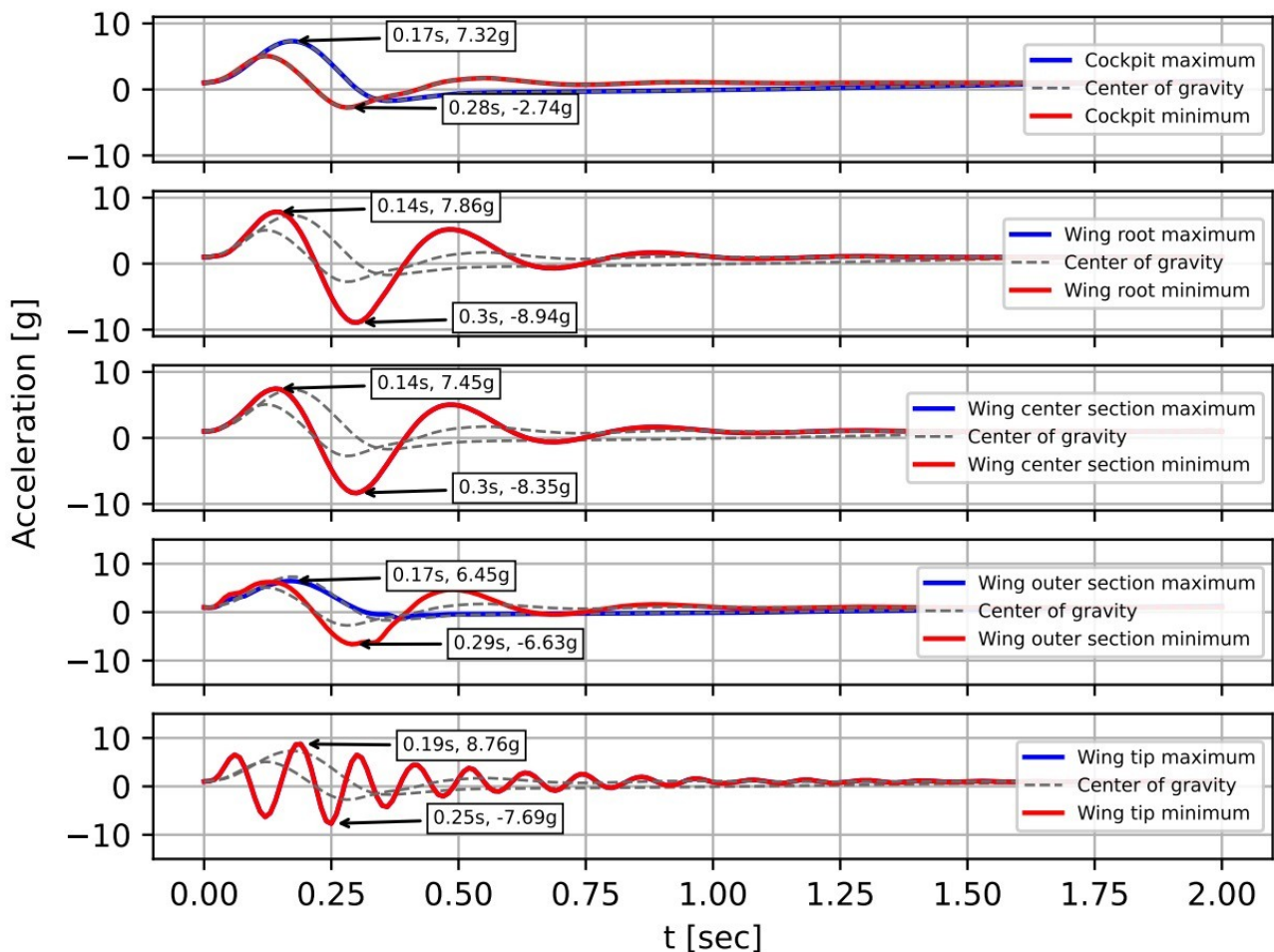


Figure 13 – Accelerations at various locations on the aircraft, vertical gust with $H = 56 \text{ m}$.

Figure 14 presents the accelerations observed for a short gust with a gradient of $H = 9 \text{ m}$. While for the center of gravity and the cockpit moderate accelerations with a peak at around $3.3g$ are observed, the curves start to oscillate at the wing root and accelerations rise to $7.9g$. A rapid increase of the accelerations can be noticed towards the outer wing, with peaks close to $100g$ on the wingtip. The reason could be an excitation of the aircraft structure by the gust. Indeed, the primary frequency of the wing tip acceleration is identified as $f \approx 17.2 \text{ Hz}$ while the first symmetric wing bending is at $f \approx 17.5 \text{ Hz}$ for the corresponding mass case.

In contrast to common misconceptions, not the acceleration but the section loads are sizing factors for the structure and the maximum of these two quantities do not always correlate. Still, the large accelerations lead to implications for two properties concerning the operational deployment of the aircraft:

Payload and Pilot limits.

The high positive and negative accelerations observed at the wing tips mean that mounting payloads at these areas would be difficult. Both the mounting and payload would need to be sized accordingly to withstand these high accelerations. Albeit attaching payloads to the wings would have an alleviating effect due to the additional inertial forces counteracting the acceleration, the resulting acceleration would still be of significant magnitude. This could be an explanation for why supersonic delta configurations similar to the FFD, such as the F-22 Raptor or the F-35 Lightning II, do not display

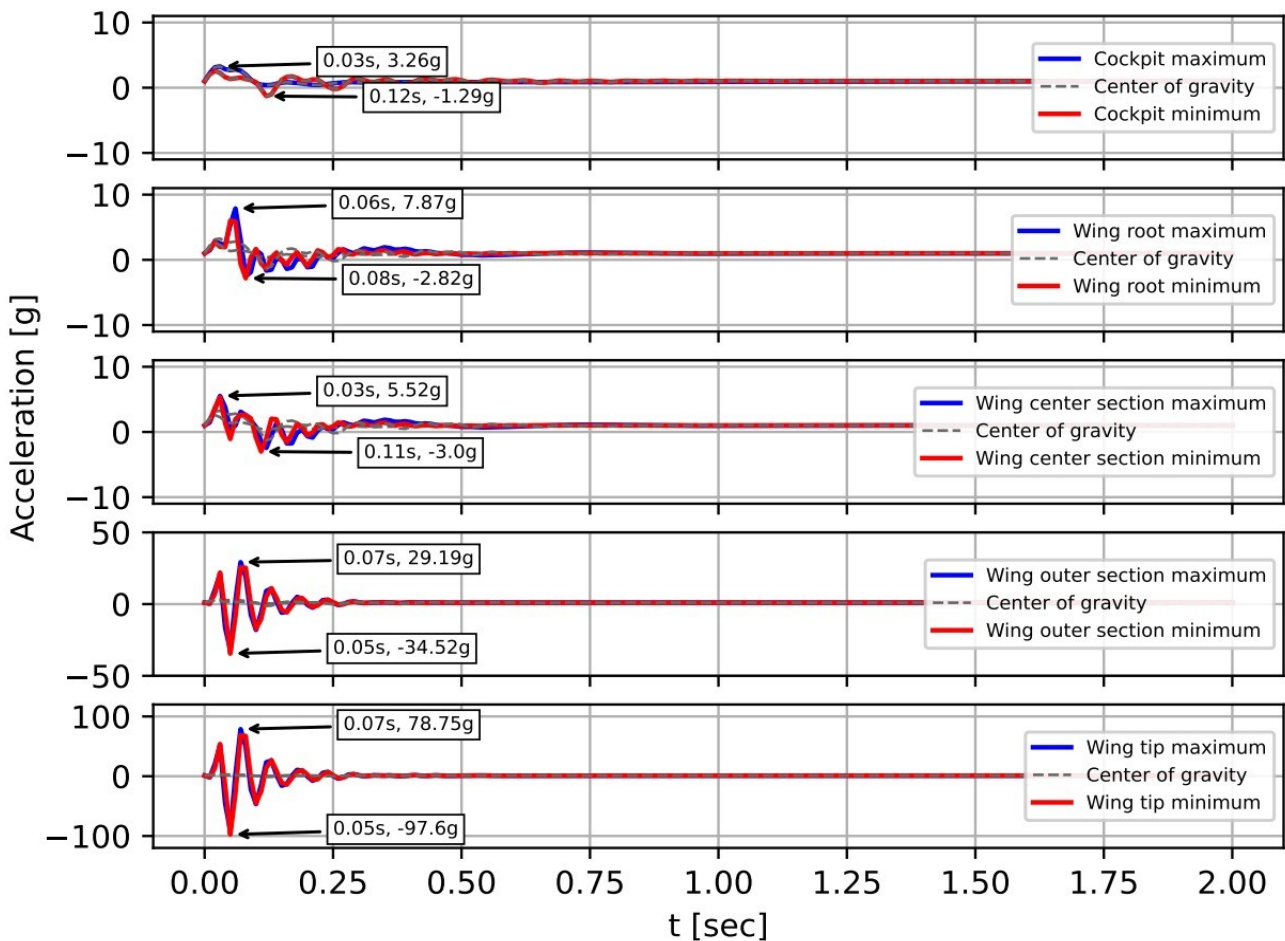


Figure 14 – Accelerations at various locations on the aircraft, vertical gust with $H = 9 \text{ m}$.

hardpoints around the wingtips to mount payloads in these areas, neither in stealth nor in the non-stealth configurations [17,18].

Although the acceleration may not directly impact the structural sizing, it does affect an essential component of the aircraft system: the pilot. As humans can bear a maximum acceleration of around $9g$ before losing consciousness (possibly slightly more depending on the exposure time), the accelerations experienced in the cockpit could thus lead to restrictions for the operation in turbulent air. Superposing the accelerations due to gust encounter and from maneuver, it becomes necessary to reduce the allowed maneuver load factor during flight in turbulent air. For example at sea level, the highest acceleration due to gust is $+6.3g$, which leaves only a small margin for the maneuver load factor with $N_{z,\max}^{\text{turbulence}} = +2.7$ instead of $N_z^{\text{max}} = +9.0$. Such limits may be adjusted based on factors as the likelihood of the gust impact, flight patterns and other variables.

4. Summary and Outlook

This work presents the findings from a comprehensive gust loads campaign for a supersonic fighter aircraft at the example of the DLR Future Fighter Demonstrator (FFD). The aeroelastic models are extended by a longitudinal flight control system, which is mandatory for meaningful results as such aircraft are typically unstable in the subsonic regime. The control system demonstrated the ability to effectively handle the worst-case gust encounter within the control surface rate limit of current generation fighter jets.

Because the military specifications partially lag behind the civil specifications concerning gust loads, the CS-25 approach with transient 1-cos gusts is adopted but without a flight profile alleviation factor. The range of gust gradients $H = 9 \dots 107 \text{ m}$ required by CS-25 was deemed satisfactory in capturing the peak section loads. However, most of the resulting section loads stayed well within the maneuver loads envelope. Comparing different methods for gust load computations, it can be concluded that for a supersonic combat configuration like the FFD, the transient gust analysis should be preferred as the quasi-steady Pratt method does not provide conservative results.

Short gust gradients may not result in large section loads, but they result in considerable accelerations on the wing tips. The investigation found that the wingtips experienced a vertical acceleration of close to $100g$. Although payload mounted on the wings might decrease some of the accelerations, the local accelerations will still be significant. This requires a suitable sizing of both the payload and attachment points or shifting all external payloads further inboard.

Even close to the center of gravity or the cockpit, the accelerations exceed the initial estimate, reaching about $7g$ during the gust impact. Additionally, the negative vertical accelerations exceed the maneuver load limit of $N_z^{\text{min}} = -3.0$, suggesting a reevaluation of the limits a human pilot can endure. Therefore, it may be necessary to limit the allowed maneuver load factor for each flight condition to avoid exceeding the structural or pilot limit when flying through turbulent air.

Note that in Figure 12 actually two maneuver load envelopes were given, one calculated with aerodynamic panel methods and one with CFD methods. Although not elaborated in the text, they showed some differences [24]. This raises the question whether using aerodynamic panel methods is justified for the gust encounter or whether CFD methods should be used in this context as well? That question will be investigated in [23].

Contact Author Email Address

mailto: arne.voss@dlr.de

Copyright Statement

The authors confirm that they, and/or their company or organization, hold copyright on all of the original material included in this paper. The authors also confirm that they have obtained permission, from the copyright holder of any third party material included in this paper, to publish it as part of their paper. The authors confirm that they give permission, or have obtained permission from the copyright holder of this paper, for the publication and distribution of this paper as part of the ICAS proceedings or as individual off-prints from the proceedings.

References

- [1] Baier J., Gust load prediction on supersonic future fighter aircraft. Bachelor Thesis, TU München & DLR Institute of Aeroelasticity, Göttingen, Germany, 2023.
- [2] Barham R., Thrust vector aided maneuvering of the YF-22 advanced tactical fighter prototype. *Biennial Flight Test Conference*, Hilton Head, SC, 1994, <https://doi.org/10.2514/6.1994-2105>.
- [3] Becker J., Gust load prediction and alleviation on a fighter aircraft. *AGARD Structures and Materials Panel*, Oberammergau, Germany, AGARD Report No.728, Sep. 1985.
- [4] Brockhaus R, Alles W, and Luckner R., *Flugregelung*. Berlin: Springer Berlin, 2010, <http://dx.doi.org/10.1007/978-3-642-01443-7>.
- [5] Brown P N, Byrne G D, and Hindmarsh A C., VODE: A variable-coefficient ODE solver. *SIAM Journal on Scientific and Statistical Computing*, vol. 10, no. 5, pp. 1038–1051, Sep. 1989, <https://doi.org/10.1137/0910062>.
- [6] Chapman R., Dynamic loading considerations in design of modern combat aircraft. *AGARD Structures and Materials Panel meeting on Loads and Requirements for Military Aircraft*, Florence, Italy, 1996.
- [7] Chen P C, and Liu D D., A harmonic gradient method for unsteady supersonic flow calculations. *Journal of Aircraft*, vol. 22, no. 5, pp. 371–379, 1985, <https://doi.org/10.2514/3.45134>.
- [8] Handojo V, and Klimmek, T, Böenlastanalyse der vorwärts gepfeilten ALLEGRA-Konfiguration. *Deutscher Luft- und Raumfahrtkongress*, Rostock, 2015.
- [9] Klimmek T., Parameterization of topology and geometry for the multidisciplinary optimization of wing structures. *CEAS 2009 - European Air and Space Conference*, Manchester, United Kingdom, 2009.
- [10] Liu D D, James D K, Chen P C, and Pototzky A S., Further studies of harmonic gradient method for supersonic aeroelastic applications. *Journal of Aircraft*, vol. 28, no. 9, pp. 598–605, 1991, <https://doi.org/10.2514/3.46070>.
- [11] Luber W G, Becker J, and Sensburg O., The impact of dynamic loads on the design of military aircraft. *AGARD Structures and Materials Panel meeting on Loads and Requirements for Military Aircraft*, Florence, Italy, 1996.
- [12] Mancini A, Zamboni J, and Moerland E, A knowledge-based methodology for the initiation of military aircraft configurations. *AIAA AVIATION 2021 FORUM*, Virtual Event, 2021, <https://doi.org/10.2514/6.2021-2789>.
- [13] Military and Government Specs & Standards, Flying qualities of piloted aircraft - MIL-STD-1797. 1990.
- [14] National Research Council, Understanding and preventing unfavorable pilot-vehicle interactions. Aeronautics and Space Engineering Board, Commission on Engineering and Technical Systems, National Research Council, Washington D.C., 1997, <http://nap.edu/5469>.
- [15] NATO Research and Technology Organisation, Flight control design – best practices. NATO Research and Technology Organisation, RTO-TR-029, Dec. 2000.
- [16] Neubauer M, and Gunther G., Aircraft loads. *RTO AVT Lecture Series on Aging Aircraft Fleets: Structural and Other Subsystem Aspects*, Sofia, Bulgaria, 2000, <https://apps.dtic.mil/sti/citations/ADP010772>.

- [17] Pike J., F-22 weapons. *GlobalSecurity.org*, 22-Jan-2016. [Online]. Available: <https://www.globalsecurity.org/military/systems/aircraft/f-22-weapons.htm>. [Accessed: 16-Oct-2023].
- [18] Pike J., F-35 joint strike fighter. *GlobalSecurity.org*, 18-May-2017. [Online]. Available: <https://www.globalsecurity.org/military/systems/aircraft/f-35.htm>. [Accessed: 16-Oct-2023].
- [19] Pratt K G, and Walker W G, A revised gust-load formula and a re-evaluation of V-G data taken on civil transport airplanes from 1933 to 1950. National Advisory Committee for Aeronautics. Langley Aeronautical Lab., Langley Field, VA, Technical Report NACA-TR-1206, 1953.
- [20] Stevens B L, Lewis F L, and Johnson E N., *Aircraft control and simulation: dynamics, controls design, and autonomous systems: dynamics, controls design, and autonomous systems*. 1st ed. Wiley, 2015, <https://doi.org/10.1002/9781119174882>.
- [21] Stradtner M, Liersch C M, and Löchert P., Multi-fidelity aerodynamic data set generation for early aircraft design phases. *AVT-366 Use of Computational Fluid Dynamics for Design and Analysis: Bridging the Gap Between Industry and Developers*, 2022.
- [22] Voß A., An implementation of the vortex lattice and the doublet lattice method. Institut für Aeroelastik, Deutsches Zentrum für Luft- und Raumfahrt, Göttingen, Germany, Technical Report DLR-IB-AE-GO-2020-137, Oktober 2020, <https://elib.dlr.de/136536/>.
- [23] Voß, A., Gust encounter of a supersonic fighter aircraft using cfd methods. *International Forum on Aeroelasticity and Structural Dynamics*, Den Haag, The Netherlands, 2024.
- [24] Voß A, and Klimmek T., Parametric aeroelastic modeling, maneuver loads analysis using CFD methods and structural design of a fighter aircraft. *Aerospace Science and Technology*, vol. 136, Mar. 2023, <https://doi.org/10.1016/j.ast.2023.108231>.
- [25] Watson G J., Eurofighter 2000 structural design criteria and design loading assumptions. *AGARD Structures and Materials Panel meeting on Loads and Requirements for Military Aircraft*, Florence, Italy, 1996.
- [26] Certification specifications for large aeroplanes CS-25, Amendment 16. European Aviation Safety Agency, 2015, <https://www.easa.europa.eu/certification-specifications/cs-25-large-aeroplanes>.
- [27] Certification specifications for normal, utility, aerobatic, and commuter category aeroplanes CS-23, Amendment 3. European Aviation Safety Agency, 2012, <https://www.easa.europa.eu/certification-specifications/cs-23-normal-utility-aerobatic-and-commuter-aeroplanes>.
- [28] JSSG-2006 Joint service specification guide aircraft structures. US Department of Defence, 1998.
- [29] MIL-A-8860B Airplane strength and rigidity general specifications. US Navy, 1987.
- [30] MIL-A-8861B Airplane strength and rigidity flight loads. US Navy, 1986.
- [31] MIL-DTL-9490E Flight control systems - design, installation and test of piloted aircraft, general specification. US Department of Defence, 2008.
- [32] MIL-F-8785C Flying qualities of piloted airplanes. US Navy, 1980.